Natural off-stoichiometry causes carrier doping in half-Heusler filled tetrahedral structures

Yonggang G. Yu*, Xiuwen Zhang, and Alex Zunger†
University of Colorado Boulder, Renewable and Sustainable Energy Institute, Boulder, Colorado 80309, USA
(Received 16 August 2016; published 3 February 2017)

The half-Heusler filled tetrahedral structures (FTSs) are zinc-blende-like compounds, where an additional atom is filling its previously empty interstitial site. The FTSs having 18 valence electrons per formula unit are an emerging family of functional materials, whose intrinsic doping trends underlying a wide range of electronic functionalities are yet to be understood. Interestingly, even pristine compounds without any attempt at impurity/chemical doping exhibit intriguing trends in the free carriers they exhibit. Applying the first principles theory of doping to a few prototype compounds in the $A^{IV}B^{X}C^{IV}$ and $A^{IV}B^{IX}C^{V}$ groups, we describe the key ingredients controlling the materials' propensity for both intrinsic and extrinsic doping: (a) The spontaneous deviations from 1:1:1 stoichiometry reflect predictable thermodynamic stability of specific competing phases. (b) Bulk ABC compounds containing 3d elements in the B position (ZrNiSn and ZrCoSb) are predicted to be naturally 3d rich. The B = 3d interstitials are the prevailing shallow donors, whereas the potential acceptors (e.g., Zr vacancy and Sn-on-Zr antisite) are ineffective electron killers, resulting in an overall uncompensated n-type character, even without any chemical doping. In these materials, the band edges are "natural impurity bands" due to non-Daltonian off-stoichiometry, such as B interstitials, not intrinsic bulk controlled states as in a perfect crystal. (c) Bulk ABC compounds containing 5d elements in the B position (ZrPtSn, ZrIrSb, and TaIrGe) are predicted to be naturally B rich and A poor. This promotes the hole-producing B-on-A antisite defects rather than B-interstitial donors. The resultant p-type character (without chemical doping) therein is "latent" for Sn and Sb; however, as the B-on-A hole-producing acceptors are rather deep, any p-type conductiveness is manifest only at high temperature or via impurity doping. In contrast, in TaIrGe (B = Ir, 5d), the prevailing hole-producing Ge-on-Ta antisite (C-on-A) is shallow, making it a real p-type compound. This general physical picture establishes the basic trends of carriers in this group of materials.

DOI: 10.1103/PhysRevB.95.085201

I. INTRODUCTION: THE FAMILIES OF HALF-HEUSLER FILLED-TETRAHEDRAL STRUCTURE COMPOUNDS WITH 18 VALENCE ELECTRONS

Nature's most succinct ternary structures belong to the 1:1:1 equiatomic ABC compounds [1–8]. They encompass two main families: (i) the eight valence-electron (octet) family [3,9] containing the groups $A^{I}B^{II}C^{V}$ (e.g., LiZnP), $A^{I}B^{III}C^{IV}$ (e.g., LiGaSi), $A^{II}B^{II}C^{IV}$ (e.g., MgSrSi), and $A^{II}B^{III}C^{III}$ (e.g., MgYGa) and (ii) the 18 valence-electron family [10–14] that appears in a few chemical groups, such as $A^{III}B^{X}C^{V}$ (e.g., ScPtSb), $A^{IV}B^{X}C^{IV}$ (e.g., ZrNiSn), $A^{IV}B^{IX}C^{V}$ (e.g., TiCoSb), and $A^{V}B^{IX}C^{IV}$ (e.g., TaIrGe [12–14]). These are "multifunctional materials" [11], due to their capacity to host a rich variety of 3d, 4d, and 5d transition metal elements and because of their appearance in numerous (over 40) crystal structure types, as summarized in Ref. [12], based on the Inorganic Crystal Structure Database (ICSD) [15]. The combination of structures and elements provides opportunities for tuning and designing electronic band structures, spin-orbit

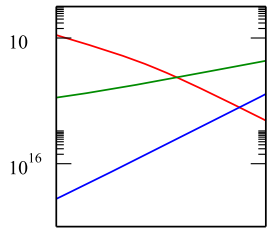
10
10^{16}

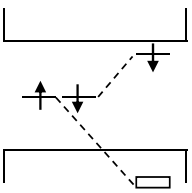

B. The chemical stability field reveals tendencies towards off-stoichiometry and identifies the leading charge neutral defects

The formation of ABC ternary under a given set of chemical potential condition with $\mu_{A,B,C} < 0$ requires that $\mu_A + \mu_B + \mu_C = H_f(ABC)$, where $H_f(ABC)$ is the compound formation energy. Projection of this equation onto the $\{\mu_A, \mu_B\}$ plane leads to a chemical potential triangle frame $\mu_A + \mu_B > H_f(ABC)$, with $\mu_{A,B} <$

IV. RESULTS: DEFECT CALCULATIONS ON ABC COMPOUNDS

A. Outline of the salient features of the method: Defect formation energy, charge transition energy, equilibrium Fermi energy, and carrier concentrations

The central quantities calculated here are (i) the defect formation energies $H(D,q,\mu,E_F)$ for various charge states q, chemical potentials μ, and Fermi energy value E_F and (ii) the defect charge transition levels $\varepsilon(D,q|q')$ between charge states q and q'.

The formation energy $H(D,q,\mu,E_F)$ for defect D in charge states q depend linearly on the atomic chemical potential $\{\mu\}$

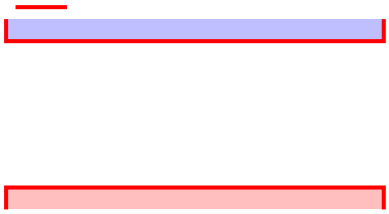

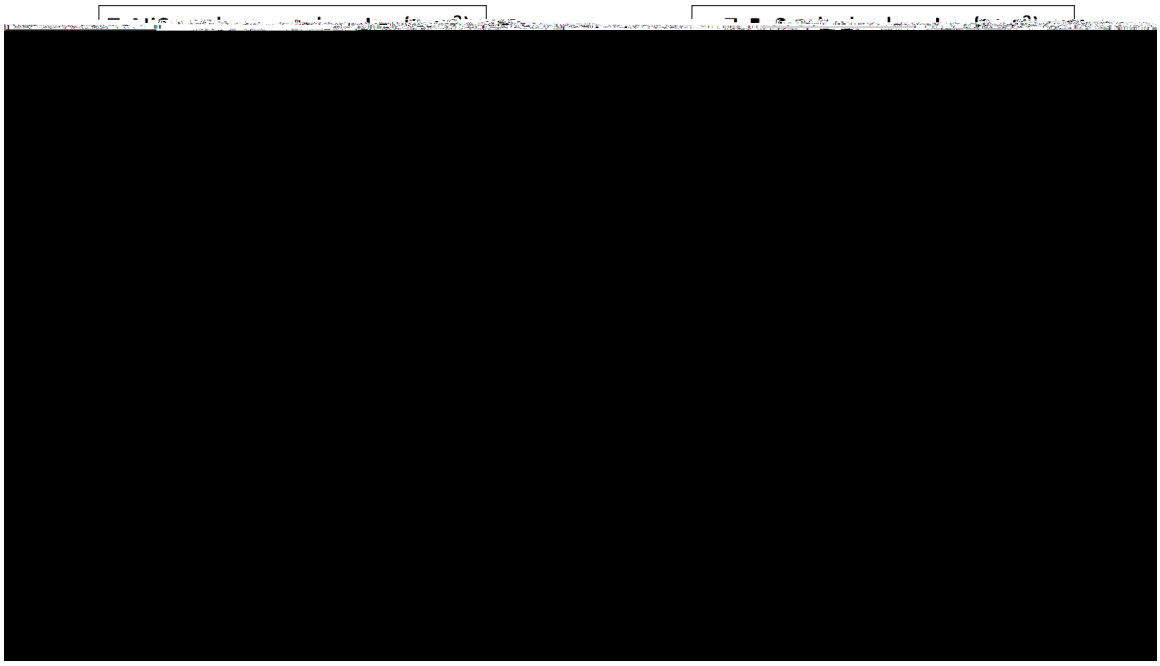

FIG. 9. Isosurface plot of the majority carrier concentrations as a function of excess chemical potentials of A and B elements within the allowed stability triangle region for four half-Haussler compounds: ZrNiSn (a) and (b), ZrPtSn (c) and (d), ZrCoSb (e) and (f), and ZrIrSb (g) and (h). The results are shown at two temperatures: at growth condition (T_g = 850 C) and at room temperature from quench after growth. The letters R and P denote the chemical potential condition, where high and low majority carrier concentration occurs, respectively. R and P represent, respectively, B-rich and B-poor condition for B = 3d compounds—ZrNiSn and ZrCoSb; C-rich and C-poor conditions for B = 5d

functional (mixing 25% of exact exchange) predicts a higher ionization level for Ni interstitial, above the CBM [Fig. 6(a)], due to effect from enhanced Hartree-Fock exchange. However, the 25% of exact exchange is only an approximation used to eliminate self-interaction corrections. We feel that our uncertainty for the Ni $(0/+1)$ charge transition level can be 0.1 eV, considering the effect of exchange on band gap opening and on eigenvalues of in-gap states. We, therefore, consider two computational scenarios allowing for 0.1 eV uncertainties, as shown by point R and L in Fig. 6(a). The two scenarios lead to completely different physical behavior in temperature dependence of carrier density. In case (i), the Ni interstitial completely ionizes and its $+(1/0)$ transition level is above the CBM [the R point in Fig. 6(a)]. Thus, the n-type carrier density remains nearly constant with temperature $(\sim 10^{20}\ \mathrm{cm}^{-3}$, the dashed red line in Fig. 10). While in case (ii), the Ni interstitial $(+1/0)$ transition level lies slightly below the CBM [e.g., $E_{CBM} - 0.07$ eV, the L point in Fig. 6(a)], the Ni interstitial only partially ionizes due to thermal excitations (10% of Ni interstitials ionize at room temperature from simulation); therefore, the carrier density increases almost linearly with temperature (the solid red line in Fig. 10). When the donor is resonant, we predict a high carrier density in ZrNiSn ($10^{19}\ \mathrm{cm}^{-3}$ at room temperature). This result from case (ii) is consistent with the observed linear T dependence of the electrical conductivity in undoped ZrNiSn samples [43,56], so it is the preferred scenario.

4. Magnetism of ionized interstitial Ni

Ni interstitials have the potential to create magnetic moments in both fully ionized and partially ionized cases. As a magnetic impurity, the Ni interstitial possesses a localized moment of $0.8\ \mu_B$ from the $x^2 - y^2$ 3d orbital. For magnetism in the dilute doping limit, it was known that p

2. The Sn-doped ZrCoSb (p type)

HSE results show that Sn-on-Sb is the dominant defect, having the lowest formation energy, but its acceptor transition level (0/1−) is rather deep (Fig. 6). Hence, the resulting hole concentration is low at room temperature and relatively high only at growth condition, 850 °C. This case illustrates a latent p-type compound, dominated by an uncompensated, deep, hole producer with low formation energy (Sn-on-Sb antisite defect), which can only generate small amount of hole carriers at room temperature (see Appendix for details).

E. Effect of A atom selection in ABC compounds with either B = 3d or B = 5d elements (the IV-X-IV and IV-IX-V groups)

Although we expect an approximately similar carrier doping behavior in the group of A^{IV}NiSn, A^{IV}PtSn, A^{IV}CoSb, and A^{IV}IrSb compounds with A^{IV} = Ti and with A^{IV} = Zr group, we are aware of the difference among the two groups. The chemical stability field of the A^{IV} = Ti group, as shown in the first column of Fig. 3, appears to be larger in area and more extended to the A-rich condition than its A^{IV} = Zr and Hf counterparts. Recently, Wambach *et al.* [36] measured the thermopower factor in the Ti-Ni-Sn compositional space using thin film growth technique with combinatorial approach.

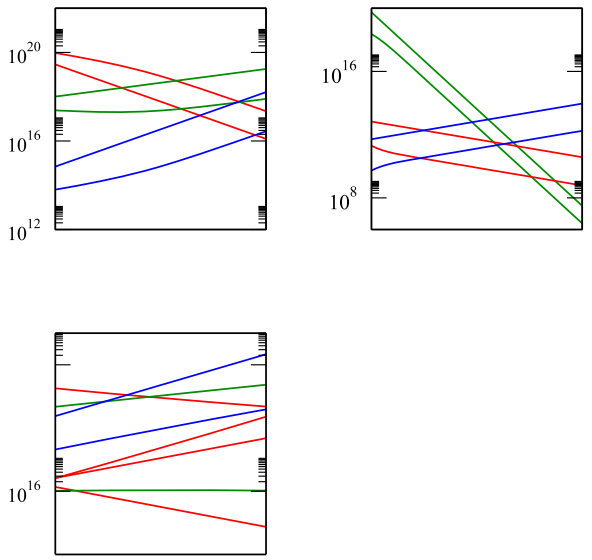
10^{20}
10^{16}
10^{12}
10^{16}
10^{8}
10^{16}

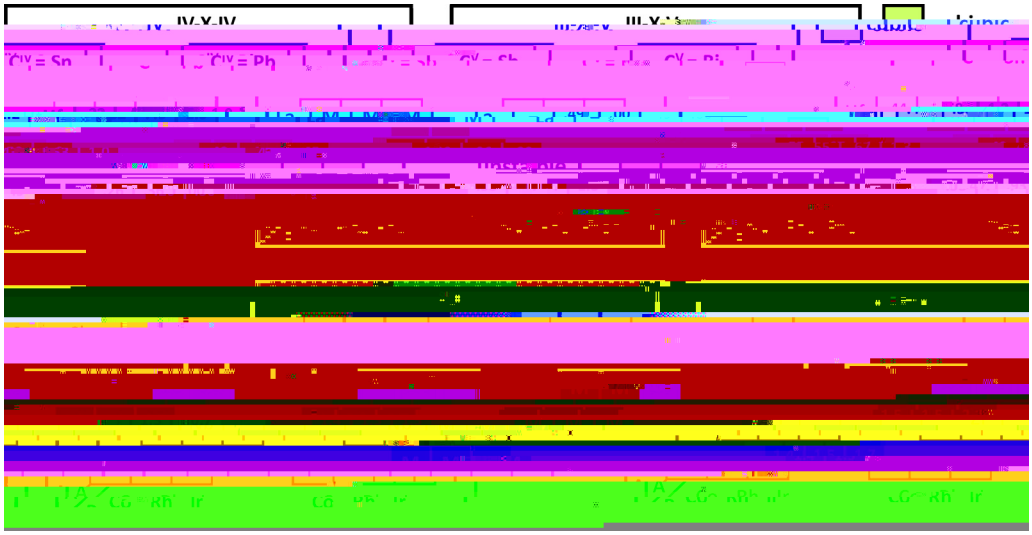

FIG. 12. Fundamental band gaps (in electron volt from HSE calculation) of a group of 18 valence-electron half-Heusler compounds in four prototype chemical groups $A^{IV}B^{X}C^{IV}$, $A^{IV}B^{IX}C^{V}$, $A^{III}B^{X}C^{V}$, and $A^{V}B^{IX}C^{IV}$. The ternary compounds with cubic structure ($F\bar{4}3m$) are nonmetal (shaded in green), whereas those in noncubic structures are metal (shaded in blue). Those that are predicted unstable are denoted by a minus sign (–).

50 cubic half-Heusler compounds reveals that the band structures are energetically unfavorable, about 0.7 eV per atom higher than the ground state (Fig. 14), indicating their non-existence.

2. Compound formation enthalpies and competing phases

The fitted elementary reference energy method (FERE [73]) in conjunction with DFT has been successfully applied to compute compound formation enthalpies in cubic half-Heusler compounds and in their computing phases (Tables II and III). The results show significant improvement over the plain GGA calculations, and are subsequently used in carrier doping studies to constrain the chemical potential stability field of the host compound.

3. Concept and computational formula for defects and doping

Defect formation energy is defined as the energy cost to create a point charged defect in an infinite lattice space (i.e., at dilute limit) through exchanging an atom and electron with the chemical reservoir and Fermi sea, respectively. To extract the defect formation energy from a finite supercell calculation, one uses the following formula

$$H_f(D,q,\mu_i,E_F) = \{E(D,q) - E_H\} \pm \sum_i n_i(\mu_i^0 + \mu_i) + q(E_V + E_F) + H_{corr} \quad \text{(A1)}$$

where $H_f(D,q,\mu_i,E_F)$ is the formation energy of defect D in charge state q under the condition of elemental chemical potential μ_i and the parametric electronic Fermi

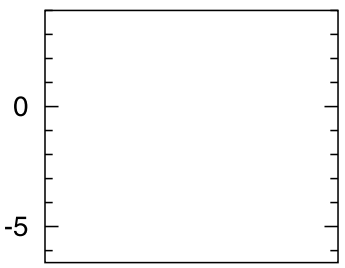
0
-5

TABLE III. Calculated formation enthalpies in units of electron volt per atom of Þve half-Heusler FTS (ZrNiSn, ZrCoSb, ZrPtSn, ZrIrSb, and TaIrGe) and their major competing phases.[a]

(a) Five half-Heusler materials			
Half-Heusler materials	H_f (eV/atom) DFT	H_f (eV/atom) DFT + FERE	H_f (eV/atom) Expt.
ZrNiSn	−0.656	−0.943	
ZrCoSb	−0.615	−0.773	
ZrPtSn	−1.032	−1.153	
ZrIrSb	−0.962	−1.082	
TaIrGe	−0.668	−0.750	
(b) Competing phases for ZrNiSn			
Compounds	H_f (eV/atom) DFT	H_f (eV/atom) DFT + FERE	H_f (eV/atom) Expt.
Zr_3Sn	−0.289	−0.850	
Zr_5Sn_3	−0.552	−1.026	−0.738
Zr_5Sn_4	−0.557	−0.982	
NiSn	−0.269	−0.332	
Ni_3Sn	−0.193	−0.271	−0.253
Ni_3Sn_2	−0.284	−0.353	−0.301
Ni_3Sn_4	−0.246	−0.306	−0.308
NiZr*	−0.452		−0.523
Ni_2Zr	−0.410		
Ni_3Zr	−0.463		
Ni_5Zr	−0.326		
$ZrNi_2Sn$	−0.517	−0.755	
$ZrNi_4Sn$	−0.350	−0.540	
Zr_2Ni_2Sn	−0.564	−0.902	
(c) Competing phases for ZrCoSb			
Compounds	H_f (eV/atom) DFT	H_f (eV/atom) DFT + FERE	H_f (eV/atom) Expt.
ZrSb	−0.695	−0.977	
$ZrSb_2$	−0.534	−0.665	−0.902
Zr_2Sb	−0.589	−1.022	−1.043
Zr_3Sb	−0.489	−0.998	−0.83
Zr_5Sb_3	−0.617	−1.012	−1.116
Zr_5Sb_4	−0.624	−0.957	
CoSb*	−0.164		−0.197
$CoSb_2$	−0.106		−0.176
$CoSb_3$	−0.142		−0.166
ZrCo*	−0.291		−0.37
$ZrCo_2$	−0.311		−0.371
Zr_2Co	−0.254		−0.274
Zr_3Co	−0.200		
(d) Competing phases for ZrPtSn			
Compounds	H_f (eV/atom) DFT	H_f (eV/atom) DFT + FERE	H_f (eV/atom) Expt.
Zr_5Sn_3	−0.552	−1.026	−0.738
Zr_5Sn_4	−0.557	−0.982	
PtSn*	−0.646		−0.609
$PtSn_2$	−0.481		−0.542
$PtSn_4$	−0.295		−0.282
Pt_2Sn_3	−0.553		−0.564
Pt_3Sn	−0.469		−0.52
ZrPt*	−1.084		−1.078
$ZrPt_3$	−1.017		
Zr_5			

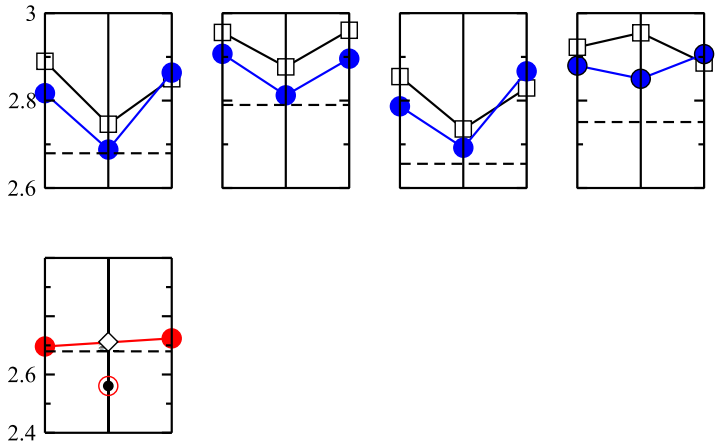
3
2.8
2.6
2.6
2.4

(Sn-on-Zr)$^{2-}$ acceptors pins E_F^{eq} closer to VBM (E_V + 0.6 eV), thus introducing holes into the host. In Fig. 22, the hole carrier density in Sn-doped ZrCoSb shows maximum at the Co-poor and Sb-poor condition (the lower right corner in the stability Þeld), because the Co-poor condition suppresses Co-interstitial donors which kill holes, while Sb-poor condition is beneÞcial to the creation of Sn-on-Sb substitution. An example for the variation of charged impurity concentration as a function of chemical potential condition is discussed in Fig. 21, which is analogous to the total impurity concentration diagram in Fig. 4.

10. Doping trends in Þve ABC compounds

We summarize in Fig. 23 our defect computational results for the dominant donors and acceptors in ZrNiSn, ZrCoSb, ZrPtSn, ZrIrSb, and TaIrGe. The characteristics of the dominant donors (or acceptors) and their primary opponents are described in terms of defect formation energy, transition levels, and resulting equilibrium carriers, which serves as the key doping information for the Þve compounds. The formation energy and carrier density are described at the equilibrium Fermi level condition.

[1] E. Parthe, Crystal Chemistry of Tetrahedral Structures (Gordon and Breach Science Publishers, New York, 1964).
[2] L. I. Berger, Semiconductor Materials (CRC Press, Boca Raton, FL, 1996).
[3] H. Nowotny and W. Siebert, Zeit. Met. 33, 391 (1941).
[4] H. Nowotny and K. Bachmayer, Monatshefte Chem. Verwandte Teile And. Wiss. 81, 488 (1950).
[5] R. Juza and F. Hund, Z. Anorg. Chem. 257, 1 (1948).
[6] R. Juza and F. Hund, Naturwissenschaften 33, 121 (1946).
[7] D. M. Wood, A. Zunger, and R. de Groot, Phys. Rev. B 31, 2570 (1985).
[8] A. E. Carlsson, A. Zunger, and D. M. Wood, Phys. Rev. B 32, 1386 (1985).
[9] S.-H. Wei and A. Zunger, Phys. Rev. Lett. 56, 528 (1986).
[10] F. Casper, T. Graf, S. Chadov, B. Balke, and C. Felser, Semicond. Sci. Technol. 27, 063001 (2012).
[11] F. Casper, R. Seshadri, and C. Felser, Phys. Status Solidi A 206, 1090 (2009).
[12] X. W. Zhang, L. P. Yu, A. Zakutayev, and A. Zunger, Adv. Funct. Mater. 22, 1425 (2012).
[13] R. Gautier, X. W. Zhang, L. H. Hu, L. P. Yu, Y. Y. Lin, T. O. L. Sunde, D. Chon, K. R. Poeppelmeier, and A. Zunger, Nat. Chem. 7, 308 (2015).
[14] F. Yan, X. W. Zhang, Y. G. Yu, L. P. Yu, A. Nagaraja, T. O. Mason, and A. Zunger, Nat. Commun. 6, 7308 (2015).
[15] ICSD, Inorganic Crystal Structure Database (Fachinformationszentrum Karlsruhe, Karlsruhe, Germany, 2013).
[16] S. Chadov, X. Qi, J. Kubler, G. H. Fecher, C. Felser, and S. C. Zhang, Nat. Mater. 9, 541 (2010).
[17] H. Lin, L. A. Wray, Y. Xia, S. Xu, S. Jia, R. J. Cava, A. Bansil, and M. Z. Hasan, Nat. Mater. 9, 546 (2010).
[18] A. Roy, J. W. Bennett, K. M. Rabe, and D. Vanderbilt, Phys. Rev. Lett. 109, 037602 (2012).
[19] S. Wang, Z. Wang, W. Setyawan, N. Mingo, and S. Curtarolo, Phys. Rev. X 1, 021012 (2011).
[20] G. J. Snyder and E. S. Toberer, Nat. Mater. 7, 105 (2008).
[21] G. J. Snyder and T. S. Ursell, Phys. Rev. Lett. 91, 148301 (2003).
[22] C. Uher, J. Yang, S. Hu, D. T. Morelli, and G. P. Meisner, Phys. Rev. B 59, 8615 (1999).
[23] K. Ishizaka, M. S. Bahramy, H. Murakawa, M. Sakano, T. Shimojima, T. Sonobe, K. Koizumi, S. Shin, H. Miyahara, A. Kimura, K. Miyamoto, T. Okuda, H. Namatame, M. Taniguchi, R. Arita, N. Nagaosa, K. Kobayashi, Y. Murakami, R. Kumai et al., Nat. Mater. 10, 521 (2011).
[24] J. Kubler, A. R. William, and C. B. Sommers, Phys. Rev. B 28, 1745 (1983).
[25] R. A. de Groot, F. M. Mueller, P. G. van Engen, and K. H. J. Buschow, 5

[43] H. Xie, H. Wang, C. Fu, Y. Liu, G. J. Snyder, X. Zhao, and T. Zhu, Sci. Rep. 4, 6888 (2014).
[44] V. V. Romaka, P. Rogl, L. Romaka, Y. Stadnyk, A. Grytsiv, O. Lakh, and V. Krayovskii, Intermetallics 35, 45 (2013).
[45] A. Zunger, Appl. Phys. Lett. 83, 57 (2003).
[46] J. P. Perdew and A. Zunger, Phys. Rev. B 23, 5048 (1981).
[47] J. Schmitt, Z. M. Gibbs, G. J. Snyder, and C. Felser, Mater. Horiz. 2, 68 (2015).
[48] F. G. Aliev, N. B. Brandt, V. V. Kozyrkov, V. V. Moshchalkov, R. V. Skolozdra, Y. V. Stadnyk, and V. K. Pecharskii, JETP Lett. 45, 684 (1987).
[49] S. Ogut and K. M. Rabe, Phys. Rev. B 51, 10443 (1995).
[50] K. Miyamoto, A. Kimura, K. Sakamoto, M. Ye, Y. Cui, K. Shimada, H. Namatame, M. Taniguchi, S. Fujimori, Y. Saitoh, E. Ikenaga, K. Kobayashi, J. Tadano, and T. Kanomata, Appl. Phys. Lett. 96, 152105 (2010).
[51] P. Larson, S. D. Mahanti, and M. G. Kanatzidis, Phys. Rev. B 62, 12754 (2000).
[52] S. Lany and A. Zunger, Phys. Rev. B 78, 235104 (2008).
[53] P. R. C. Kent and A. Zunger, Phys. Rev. Lett. 86, 2613 (2001).
[54] D. T. Do, S. D. Mahanti, and J. J. Pulikkoti, J. Phys.: Condens. Matter 26, 275501 (2014).
[55] K. Miyamoto et al., Appl. Phys. Express 1, 081901 (2008).
[56] V. A. Romaka, P. Rogl, V. V. Romaka, Y. V. Stadnyk, E. K. Hlil, V. Y. Krajovskii, and A. M. Horyn, Semiconductors 47, 892 (2013).